Journal of Colloid and Interface Science 513 (2018) 409–417

Contents lists available at ScienceDirect

Journal of Colloid and Interface Science

journal homepage: www.elsevier.com/locate/jcis

Regular Article

Stabilization of axisymmetric liquid bridges through vibration-induced pressure fields

M. Haynes [a], E.J. Vega [b,*], M.A. Herrada [c], E.S. Benilov [a], J.M. Montanero [b]

[a] Department of Mathematics, University of Limerick, Limerick V94 T9PX, Ireland
[b] Depto. de Ingeniería Mecánica, Energética y de los Materiales and Instituto de Computación Científica Avanzada (ICCAEx), Universidad de Extremadura, E-06006 Badajoz, Spain
[c] Depto. de Mecánica de Fluidos e Ingeniería Aeroespacial, Universidad de Sevilla, E-41092 Sevilla, Spain

GRAPHICAL ABSTRACT

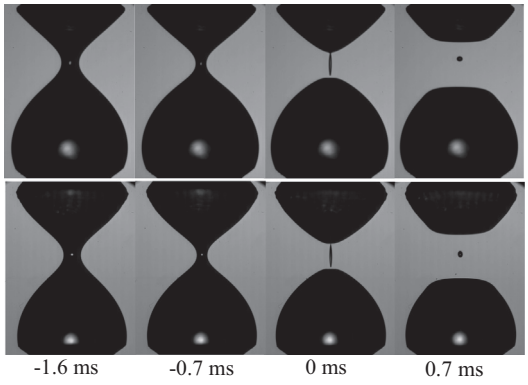

ARTICLE INFO

Article history:
Received 12 September 2017
Revised 16 November 2017
Accepted 17 November 2017
Available online 21 November 2017

Keywords:
Liquid bridge
Stabilization
High frequency vibration
Mass transfer

ABSTRACT

Previous theoretical studies have indicated that liquid bridges close to the Plateau-Rayleigh instability limit can be stabilized when the upper supporting disk vibrates at a very high frequency and with a very small amplitude. The major effect of the vibration-induced pressure field is to straighten the liquid bridge free surface to compensate for the deformation caused by gravity. As a consequence, the apparent Bond number decreases and the maximum liquid bridge length increases. In this paper, we show experimentally that this procedure can be used to stabilize millimeter liquid bridges in air under normal gravity conditions. The breakup of vibrated liquid bridges is examined experimentally and compared with that produced in absence of vibration. In addition, we analyze numerically the dynamics of axisymmetric liquid bridges far from the Plateau-Rayleigh instability limit by solving the Navier-Stokes equations. We calculate the eigenfrequencies characterizing the linear oscillation modes of vibrated liquid bridges, and determine their stability limits. The breakup process of a vibrated liquid bridge at that stability limit is simulated too. We find qualitative agreement between the numerical predictions for both the stability limits and the breakup process and their experimental counterparts. Finally, we show the applicability of our technique to control the amount of liquid transferred between two solid surfaces.

* Corresponding author.
E-mail address: ejvega@unex.es (E.J. Vega).

https://doi.org/10.1016/j.jcis.2017.11.056
0021-9797/

1. Introduction

Liquid bridges occur and play a relevant role both in nature [1,2] and in many industrial applications, such as materials engineering [3], powder granulation [4] and flow in porous media [5]. When the solid supports are surfaces parallel to each other, the liquid bridge becomes a relatively simple configuration, commonly used as a testbed to study surface tension-driven phenomena. The complex dynamics of the liquid meniscus formed next to the slipping triple contact lines may significantly affect the liquid bridge behavior. The problem is simplified when the solid surfaces are disks of the appropriate size, so that the contact lines anchor to their sharp edges. This specific configuration has turned nowadays into a model system to study complex phenomena on free surfaces.

There are numerous interfacial phenomena that can be studied using liquid bridges. A good example is the instability of a constrained capillary surface under different types of perturbations [6]. It is well known that the maximum length of a weightless cylindrical bridge supported by two disks of the same diameter equals the disk circumference (the Plateau-Rayleigh stability limit) [7]. The gravitational force deforms the liquid column overcoming the resistance offered by the surface tension, which reduces the maximum slenderness (length in terms of the disk diameter). In addition, the magnitude of the gravitational force relative to that of the surface tension force scales with the disk diameter squared, which limits the disk size too. As a consequence, the volume of liquid bridges with slendernesses greater than unity cannot exceed on earth some tens of cubic millimeters. This limitation is of importance in a number of practical problems, including the classical floating zone technique used for crystal growth and purification of high melting-point materials [8], printing processes [9], and capillary feeders [10].

Liquid bridges can be stabilized if the effect of gravity is somehow compensated for. A number of methods have been proposed to this end. A simple possibility is to immerse the liquid bridge in a density-matched liquid bath (the Plateau-tank technique) so that the stability problem becomes fully equivalent to that of a liquid bridge under microgravity conditions. Using this configuration, the Plateau-Rayleigh stability limit has been overcome by enclosing the liquid bridge between elliptical disks [11], or by applying axial electric fields [12,13]. This stability limit has also been suppressed by controlling the bridge shape with the radiation pressure of an ultrasonic wave [14] or the optical-radiation pressure of a continuous laser wave [15]. Non-Newtonian effects can also enable the formation of stable liquid columns with lengths well in excess of the supporting disk circumference [16]. Small pressure gradients along the interface due to the slight imbalance between the densities of the liquids can be cancelled if the outer bath moves upwards at the appropriate speed [17,18]. A similar effect is produced by a closed-flow in both the encapsulating liquid and the bridge [19].

Both the linear and non-linear dynamics of the Plateau-tank configuration is considerably different from that of a liquid bridge in air due to the non-negligible contribution of the surrounding liquid bath. Different methods have been considered to reduce the effect of the gravitational force on a liquid bridge suspended in air. A simple alternative is to make the liquid drop rest on a lower supporting disk of diameter smaller than that of the upper one [20]. In this way, the triple contact line anchorage produces a deformation opposite of that caused by gravity, which increases the maximum slenderness. Paramagnetic liquid bridges with slendernesses very close to the Plateau-Rayleigh stability limit were formed using magnetic levitation [21,22]. Pure and leaky dielectric liquid bridges surrounded by air can be stabilized beyond that limit in the presence of an electric dc field [23]. The growth of the axisymmetric capillary mode responsible for the breakup of liquid bridges in low gravity was suppressed with both acoustic radiation pressure [24] and active electrostatic stabilization [25]. Interestingly, the stabilization caused by an axial outer liquid stream [17,18] cannot be produced by a gas current. In this case, a recirculation cell appears in the bulging part of the liquid bridge, which has a destabilizing effect independently of the gas stream direction [26,27]. A similar effect is caused by the thermal (Marangoni-buoyant) convection in liquid bridges with high Prandtl numbers [28].

Very recently [29], a method has been proposed to stabilize liquid bridges in air and close to the Plateau-Rayleigh stability limit. In this method, the upper disk is vibrated at a frequency f much higher than the inverse of the capillary time t_0, and with an amplitude a much smaller than the supporting disk radius R. In the limit $(ft_0)^{-1}, a/R \ll 1$, the effect of the disk vibration reduces to a pressure field that straightens the free surface shape. If the vibration frequency or amplitude is appropriately adjusted, the Plateau-Rayleigh stability limit can be reached for non-zero Bond numbers.

The primary goal of the present paper is to show experimentally that the method described above can indeed stabilize liquid bridges under normal gravity conditions. In Ref. [29], an analytical study was conducted for liquid bridges asymptotically close to the Plateau-Rayleigh stability limit [29]. Here, we extent that analysis to arbitrary axisymmetric shapes from numerical simulations of the Navier-Stokes equations. In addition, we describe both numerically and experimentally the breakup of vibrated liquid bridges.

2. Theoretical model

The configuration considered in this work (Fig. 1) consists of an isothermal mass of liquid of volume $\mathcal{V}$, held by the surface tension force between two parallel and coaxial disks of radius R which are placed a distance L apart. The liquid bridge density, viscosity and surface tension are ρ, μ, and σ, respectively. The surrounding gas density and viscosity are much smaller than those of the liquid, so that they do not significantly affect the liquid bridge dynamics. The liquid is subjected to the action of the axial gravitational force of magnitude g per unit mass. The upper disk is vibrating harmonically with an amplitude a and frequency f.

We use the disk radius R and the capillary time $t_0 \equiv (\rho R^3/\sigma)^{1/2}$ as the characteristic length and time, respectively. The problem can be characterized in terms of the following dimensionless parameters: the slenderness $\Lambda \equiv L/(2R)$, the reduced volume $V \equiv \mathcal{V}/(\pi R^2 L)$ (defined as the ratio of the physical volume $\mathcal{V}$ to the volume of a cylinder of length L and radius R), the Bond number $B \equiv \rho g R^2/\sigma$, the Ohnesorge number $\mathrm{Oh} \equiv \mu(\rho\sigma R)^{-1/2}$, the upper disk vibration amplitude $A \equiv a/R$, and frequency $\Omega \equiv 2\pi f t_0$. These last two quantities can be grouped into the dimensionless number $W \equiv \Omega A$, which measures the relative importance of the pressure due to the upper disk vibration versus the capillary pressure.

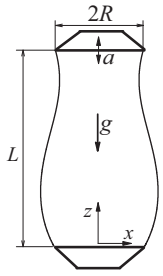

Fig. 1. Geometry and coordinate system for the liquid bridge.

For a sufficiently large frequency Ω and small amplitude A, the liquid bridge dynamics can be seen as the superposition of a fast and slow motion (the method of multiple scales) [29]. In the asymptotic limit $A \ll 1$ and $\Omega \gg 1$, the former vanishes and the latter satisfies the equations

$$(ru)_r + rw_z = 0, \tag{1}$$

$$u_T + uu_r + wu_z = -p_r + C[u_{rr} + (u/r)_r + u_{zz}], \tag{2}$$

$$w_T + uw_r + ww_z = -p_z + C[w_{rr} + w_r/r + w_{zz}], \tag{3}$$

where r and z are the radial and axial cylindrical coordinates, respectively, T is the slow time, the subscripts r, z, and T denote partial derivatives with respect to those variables, u and w are the radial and axial velocity components, respectively, and p is the (hydrostatic) reduced pressure plus the contribution $\frac{1}{4}|\nabla q|^2$ due to the vibration-induced pressure field [29]. Here, $q(r,z;T) \equiv -W^{-1}p_s$, where $p_s(r,z;T)$ is the amplitude of the zeroth order solution for the pressure field [29].

The above equations are integrated considering the regularity conditions $u = w_r = p_r = 0$ at the symmetry axis $r = 0$, the non-slip boundary condition $u = w = 0$ at the solid surfaces $z = 0$ and 2Λ, as well as the kinematic compatibility

$$F_T + F_z w - u = 0, \tag{4}$$

and the equilibrium of normal and tangential stresses

$$p + \frac{1}{4}|\nabla q|^2 - B\,z - \hat{\mathcal{C}} - \frac{2C[u_r - F_z(w_r + u_z) + F_z^2 w_z]}{1 + F_z^2} = 0, \tag{5}$$

$$[1 - F_z^2](w_r + u_z) + 2F_z(u_r - w_z) = 0 \tag{6}$$

at the free surface $r = F(z,T)$. In the above equation,

$$\hat{\mathcal{C}} = \frac{1 + F_z^2 - FF_{zz}}{F(1 + F_z^2)^{3/2}} \tag{7}$$

is twice the local mean curvature of the free surface. These boundary conditions must be complemented with the anchoring conditions at the disk edges,

$$F = 1 \quad \text{at } z = 0, 2\Lambda. \tag{8}$$

Also, the nondimensional volume is prescribed and conserved; namely,

$$\int_0^{2\Lambda} F^2\, dz = 2\Lambda V. \tag{9}$$

The vibration-induced pressure field $q(r,z;T)$ satisfies the following boundary-value problem:

$$\nabla^2 q = 0, \tag{10}$$

$$q_r = 0 \quad \text{at } r = 0, \qquad q = 0 \quad \text{at } r = F(z,T), \tag{11}$$

$$q_z = 0 \quad \text{at } z = 0, \qquad q_z = -W \quad \text{at } z = 2\Lambda. \tag{12}$$

For liquid bridges close to the Plateau-Rayleigh stability limit ($\Lambda \simeq \pi, V \simeq 1$ and $B \simeq 0$), neutral stability occurs if [29]

$$\frac{\pi^2 V}{\Lambda^2} - 1 = \left[\frac{9}{\sqrt{2}}\frac{\Lambda^2}{\pi^2}\left(B - \frac{kW^2}{8\Lambda}\right)\right]^{2/3} + \frac{3}{2}\left(\frac{\pi}{\Lambda} - 1\right)^2, \quad k \simeq 0.024794. \tag{13}$$

This expression reduces to that derived in Ref. [20] for $W = 0$. Fig. 2 shows the maximum slenderness calculated from (13) as a function of W for different Bond numbers. The vibration stabilizes the liquid bridge until the Plateau-Rayleigh stability limit ($\Lambda = \pi$) is reached. From this point on, the vibration has a destabilizing effect because the pressure field overcompensates for the effect of gravity. Eq. (13) shows that the upper disk vibration reduces the "effective" Bond number as $B \to B - kW^2/(8\Lambda)$. Therefore, the comparison between B and $kW^2/(8\Lambda)$ establishes the importance of the vibration stabilizing effect versus the gravitational destabilizing one. This consistent with the fact $q \sim W$, and therefore the term $1/4\,|\nabla q|^2$ in Eq. (6), accounting for the effect of the vibration-induced pressure field, scales as W^2. One concludes that the physical interpretation of $\widetilde{W} = kW^2/8$ ($\Lambda \sim 1$) is clearer than that of W. For this reason, we will use the former as independent governing parameter in the rest of our analysis. Therefore, the problem will be formulated in terms of the set of parameters $\{\Lambda, V, B, \mathrm{Oh}, \widetilde{W}\}$.

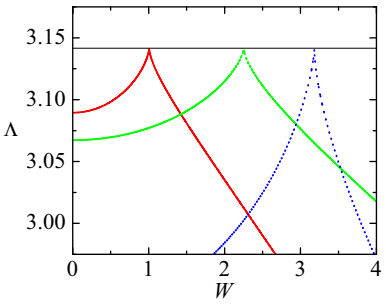

Fig. 2. Maximum slenderness calculated from Eq. (13) for $V = 1$ as a function of W for $B = 0.001$ (red solid line), 0.005 (green dashed line) and 0.01 (blue dotted line). The horizontal line is $\Lambda = \pi$. (For interpretation of the references to color in this figure legend, the reader is referred to the web version of this article.)

Eq. (13) is only valid for Bond numbers much smaller than unity. To verify this condition, experiments on Earth must be conducted with submillimeter liquid bridges, which entails important technical difficulties. In this paper, we extend the asymptotic stability analysis in Ref. [29] by numerically solving the above theoretical model for axisymmetric liquid bridges far away from the Plateau-Rayleigh stability limit. Eqs. (1)–(10) are solved with the numerical method proposed in Ref. [30].

3. Experimental method

3.1. Experimental setup

Fig. 3 shows the experimental setup used in the present work. A liquid bridge was formed between two parallel and coaxial disks (A and B) of the same radius $R = 1$ mm. The lower disk had an orifice 200 μm in diameter, which was used to feed and remove liquid by using a syringe pump connected to a stepping motor. The upper disk was fixed to a piezocomposite actuator (PSt 1000/10/7 VS18, Piezosystemjena) (C) connected to a power amplifier (LE 150/1000 EBW, Piezosystemjena). Harmonic vibrations of the upper disk were

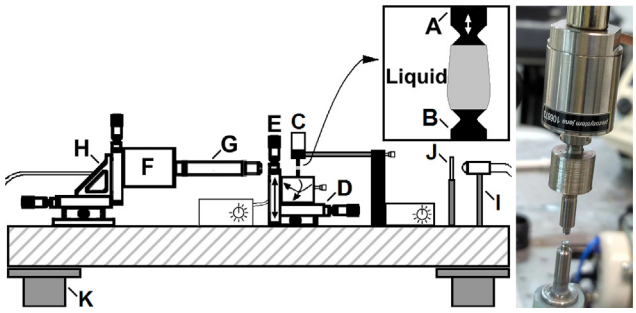

Fig. 3. Experimental setup: upper rod (A), bottom rod (B), piezocomposite actuator (C), orientation system (D), motorized stage (E), camera (F), optical lenses (G), triaxial translation stage (H), optical fiber (I), frosted diffusor (J), and anti-vibration isolation system (K).

produced with a 10-MHz function and arbitrary waveform generator (Agilent, LXI) connected to the power amplifier. The frequency of the vibration could be precisely controlled by the experimenter. However, the amplitude is the result of electro-mechanical transfer function which depends not only on the gain of the power amplifier but also on both the mass connected to the actuator and rigidity of that connection. The lower disk was fixed to a high-precision orientation system (D) to ensure the correct alignment with the upper one. This system was joined to a vertical motorized stage (Z825B connected to TDC001, scThorlabs) (E) to set the distance between the disks. The lower disk speed could be selected within the range 0.003–2.6 mm/s.

We recorded digital images of the liquid bridge at 30 frames per second using a CCD camera (AVT Stringay F-125B) (F). The images consisted of 1280 × 960 pixels, and were acquired with an exposure time of 25 μs. The camera was equipped with a telecentric objective (G) providing a magnification of approximately 7.16 μm/pixel. The liquid bridge was focused displacing the camera both horizontally and vertically by using a triaxial translation stage (H). We illuminated the fluid configuration from the back with cool white light provided by an optical fiber (I). A uniformly lit background was obtained by locating a frosted diffuser (J) between the optical fiber and the fluid configuration. We checked that the configuration was axisymmetric by acquiring images with an auxiliary CCD camera (not shown in Fig. 3) whose optical axis was perpendicular to that of the main camera. All the experimental devices were mounted on an optical table, which rested on a pneumatic anti-vibration isolation system (K). To analyze both the vibration of the upper disk and the liquid bridge breakup, images were acquired with a high-speed video camera (Photron, FASTCAM SA5). We used a sub-pixel resolution technique [31] to detect the contours in the images.

Experiments were conducted using two silicone oils (see Table 1) because their surface tensions are fairly insensitive to contamination. In fact, interfaces with higher surface tensions become contaminated very easily (especially when working with liquid bridges [32]), and the effects of that contamination may be comparable with the (small) pressure field effect. Those surface tensions were measured with the Theoretical Image Fitting Analysis (TIFA) method [33], while the rest of the liquid properties were taken from the manufacture's specifications. We selected liquids with low and moderate viscosities to examine the influence of this parameter. The ratio ρ/σ (and therefore B and $\widetilde{W}$) takes very similar values in the two liquids.

Before conducting the experiments, the actuator was calibrated. For this purpose, images of the upper disk vibrating without the liquid bridge were acquired with a high-speed video camera. The actuator calibration was conducted without the liquid bridge to accurately detect the position of the disk edge in the images. A harmonic function was fitted to the detected positions to measure both the amplitude and frequency of the oscillation. Fig. 4 shows the displacement $z_d(t)$ of the upper disk and the fit to the measured values in that case. The fitted frequency differed in less than 0.01% with respect to the value prescribed in the experiment. The analysis shown in the figure was repeated several times in the course of the experiments to make sure that the amplitude did not change due to possible mechanical mismatches. Submicrometer oscillation amplitudes were obtained in all the cases analyzed except for frequencies close to the resonance ones. As mentioned above, these frequencies are not intrinsic properties of the shaker, because they also depend on both the mass of the elements connected to it and the type of connection used. Therefore, a small shift of the shaker resonance frequency may take place when the liquid bridge hangs on the upper disk, which might result in a significant variation of the vibration amplitude. For this reason, the value of this quantity measured from the actuator calibration could not be used for comparison with theoretical results. Alternatively, we estimated the dimensionless amplitude value $\widetilde{W}$ in the experiments by fitting the liquid bridge numerical contour to the experimental one. The deviations obtained in the experiments shown in Section. 4.1 with respect to the vibration amplitude measured in the actuator calibration (without the liquid bridge) were around 30%.

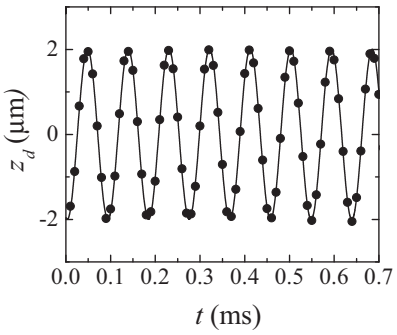

Fig. 4. Displacement of the upper disk $z_d(t)$ (symbols) and the fit $z_d = a\cos(2\pi ft + \varphi)$ to the measured values.

We could not reproduce oscillation amplitudes larger than about 2 μm at frequencies larger than around 11 kHz because the vibration unhooked the disk after some time. Consequently, we conducted the experimental runs described below with that amplitude and frequency. The corresponding results are presented in Section. 4.1. Also, we conducted a single experiment with an amplitude $a = 5.0$ μm and at a frequency $f = 13.2$ kHz to clearly appreciate the vibration effects on the liquid bridge breakage process. Images of that process are shown in Section. 4.2.

3.2. Experimental procedure

In order to determine the liquid bridge stability limit, the following steps were taken. The disks were located at a short distance to fill with liquid the gap between them. The disks were moved apart by displacing the lower disk until a slender liquid bridge was formed. Liquid was injected until the bridge dimensionless volume took a value around unity. In the experiments with vibration, the actuator was switched on. Then, the disks were moved apart by displacing the lower disk at 3.5 μm/s, while liquid was injected at 0.04 ml/h to keep the initial dimensionless volume approximately constant. Images of the liquid bridge were acquired during this quasi-static stretching process. The process was stopped when the liquid bridge broke up. An image of the liquid bridge was processed with the TIFA method [34] to determine the surface tension. The last liquid bridge image before breakup was processed to measure both the volume and distance between the two disks. The same experimental run was conducted with and

Table 1
Properties of the working liquids at 20 °C.

Liquid	ρ (kg·m^{-3})	σ (mJ/m^2)	μ (mPa·s)	Oh
1 cSt silicone oil	818	17 ±1	0.82	0.00691
35 cSt silicone oil	957	20 ±1	33	0.237

without the upper disk vibration to study the influence of the vibration-induced pressure field on the stability limit.

We also analyzed the influence of the upper disk vibration on the liquid bridge breakup process in a single experiment with an amplitude $a = 5.0$ μm and at frequency $f = 13.2$ kHz. In this case, a liquid bridge with a fixed slenderness was formed. The liquid was withdrawn with the pump until the volume reached a value close to that of the minimum volume stability limit. The actuator was switched on. Then, we let the liquid evaporate so that the bridge broke up spontaneously. Images of the process were recorded with the high-speed video camera. The same experimental procedure was followed without the upper disk vibration.

4. Results

4.1. Equilibrium shapes and stability

It is well known that liquid bridges become unstable due to the growth of the first axisymmetric oscillation mode for a wide range of experimental conditions [35]. In this work, we will restrict our analysis to those conditions. Fig. 5 shows both the damping factor and oscillation frequency characterizing the first axisymmetric oscillation mode as function of liquid bridge slenderness while the rest of parameters remain fixed. Without vibration, the oscillation frequency vanishes and the damping factor curve splits into two branches (only the dominant one is plotted) for $\Lambda \simeq 1.78$. The dominant branch behind the curve split decreases very sharply. The numerical method fails to calculate the equilibrium shape very close to the stability limit, so the marginal stability point had to be determined by extrapolation (this point is expected to be located very close to the end of that curve). Interestingly, the damping factor does not monotonically decrease as the slenderness increases. On the contrary, there is a small interval of Λ before the split of the damping factor curve where the liquid bridge stabilizes as Λ increases. This effect has been previously observed close to the minimum volume stability limit [36], and must be attributed to gravity because it does not appear in cylindrical shapes [37]. The liquid bridge vibration does not significantly affect the eigenfrequency for slendernesses smaller than that of the split point. However, it produces an almost constant lateral displacement of the dominant branch between the split and the neutral stability point. As a consequence, liquid bridges with slendernesses within the interval $1.8 \lesssim \Lambda \lesssim 1.83$ are stabilized by the upper disk vibration for $\widetilde{W} = 5.24 \times 10^{-3}$. The fact that the damping factor far from the stability limit is not significantly affected by the disk vibration implies that the stabilization effect cannot be anticipated from the damping of perturbations in stable shapes.

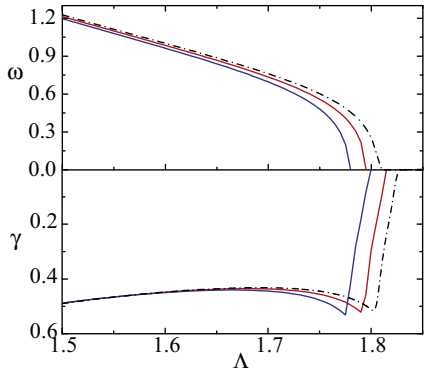

Fig. 5. Damping factor γ and oscillation frequency ω of the first axisymmetric oscillation mode calculated as function of liquid bridge slenderness Λ for $\widetilde{W} = 0$ (blue solid line), 2.86×10^{-3} (red dashed line), and 5.24×10^{-3} (black dashed-dot line). The values of the rest of governing parameters are $V = 1, B = 0.478$, and $\mathrm{Oh} = 0.237$. (For interpretation of the references to color in this figure legend, the reader is referred to the web version of this article.)

Fig. 6-left shows the free surface position for the same liquid bridge with and without the vibration-induced pressure field. The lines and symbols correspond to the experimental and numerical contours, respectively. The difference between the volumes enclosed by the two curves is smaller than 0.03%. The numerical results perfectly fit the experimental contour in the absence of vibration. As can be observed, the vibration-induced pressure field partially compensates for the effect of gravity on the liquid bridge equilibrium shape. The upper disk vibration reduces the liquid bridge deformation, which slightly decreases the average free surface curvature (Fig. 6-right).

In the absence of vibration, the local mean curvature $\hat{C}(z)$ of the free surface is a linear function of the axial coordinate z [29]. For vibrated liquid bridges with $\Lambda \gtrsim 1, \hat{C}(z)$ exhibits a quasi-linear dependence with respect to z in the major part of the liquid bridge (Fig. 6-right), where the vibration-induced pressure magnitude $\frac{1}{4}|\nabla q|^2$ takes very small values (Fig. 7). The difference between the vibration and non-vibration cases concentrates near the upper disk, where $\frac{1}{4}|\nabla q|^2$ increases up to values on the order of B (Fig. 7). The curves $\hat{C}(z)$ remain practically parallel in the rest of the liquid bridge. The slope B_{eff} of the linear function $\hat{C}(z) = \hat{C}_0 - B_{\mathrm{eff}} z$ fitted to the experimental values can be regarded as the effective Bond number accounting for both gravity and the vibration-induced pressure field. Fig. 8 shows the values of B_{eff} measured with and without vibration. As can be observed, B_{eff} slightly decreases due to the vibration-induced pressure field. The effect on the curvature slope decreases as the liquid bridge slenderness increases. This does not imply that the shape of slender liquid bridges is less affected by vibration because these bridges are more sensitive to variations of the Bond number than the short ones. The decrease of the effective Bond number is one order of magnitude larger than the $\widetilde{W}$ value.

Using the experimental procedure described in Section. 3.2, the maximum slenderness of 1 and 35-cSt silicone oil liquid bridges with volumes around unity was determined with and without vibration. As mentioned in Section. 3.1, the ratio ρ/σ takes practically the same value for the two working liquids, and therefore both B and $\widetilde{W}$ are practically constant when the vibration amplitude and frequency are fixed. However, $B \gg \widetilde{W}$, and therefore small variations of B may produce effects comparable with those caused by the vibration-induced pressure field. In order to collect all the experimental data in a single Λ against V graph, we used the Taylor expansion

$$\Lambda(1+\delta V, \overline{B}, \widetilde{W}) \simeq \Lambda(1+\delta V, \overline{B}+\delta B, \widetilde{W}) - \delta B \left.\frac{\partial \Lambda}{\partial B}\right|_{(1,\overline{B},0)} - \delta B \delta V \left.\frac{\partial^2 \Lambda}{\partial B \partial V}\right|_{(1,\overline{B},0)} - \delta V^2 \left.\frac{\partial^2 \Lambda}{\partial V^2}\right|_{(1,\overline{B},0)}, \tag{14}$$

where $\overline{B}$ is the Bond number averaged over all the experimental realizations, and $\delta V, \delta B, \widetilde{W}$ are assumed to be much smaller than unity. The values $\Lambda(1+\delta V, \overline{B}+\delta B, \widetilde{W})$ were measured in the experiments, while the Taylor expansion coefficients were evaluated numerically with the method proposed in Ref. [35]. In this way, the stability limit $\Lambda(V)$ could be approximately obtained for fixed values $\overline{B}$ and $\widetilde{W}$ of the Bond number and vibration magnitude, respectively.

Fig. 9 shows the maximum slenderness of 1 and 35-cSt silicone oil liquid bridges with and without vibration. When the upper disk vibrates, the maximum slenderness increases in around 0.03–0.1

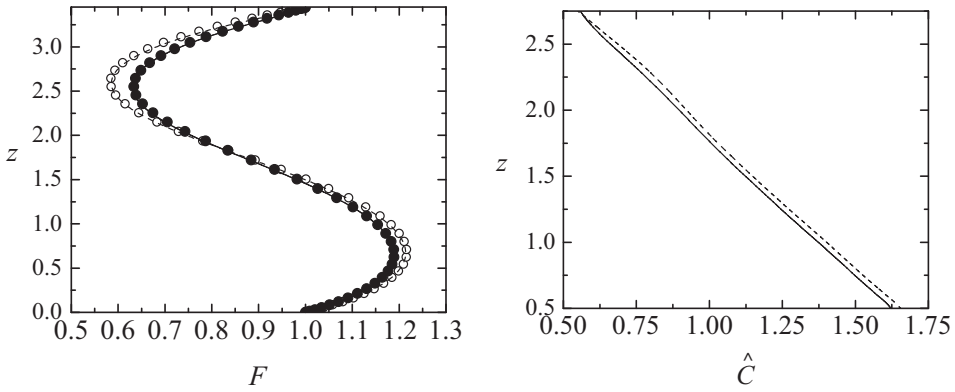

Fig. 6. Free surface position $F(z)$ (left) and local mean curvature $\hat{C}(z)$ (right) for $\Lambda = 1.722, V = 0.8893, B = 0.4822$ and $\mathrm{Oh} = 0.237$. The dashed lines and open symbols are the experimental and numerical results for $\widetilde{W} = 0$, respectively. The solid lines and solid symbols are the experimental and numerical results for $\widetilde{W} = 5.24 \times 10^{-3}$ ($W = 1.3$), respectively.

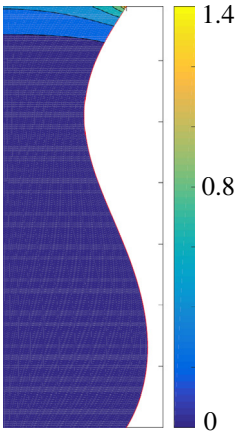

Fig. 7. Vibration-induced pressure magnitude $\frac{1}{4}|\nabla q|^2$ calculated for $\Lambda = 1.722, V = 0.8893, B = 0.4822, \mathrm{Oh} = 0.237$ and $\widetilde{W} = 5.24 \times 10^{-3}$ ($W = 1.3$).

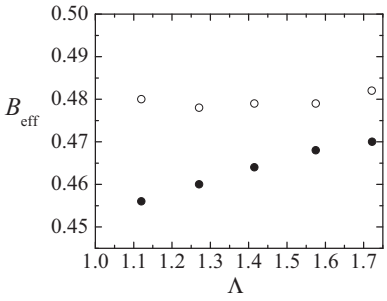

Fig. 8. Experimental values of the effective Bond number B_{eff} as a function of Λ for $\mathrm{Oh} = 0.237$. The open and solid symbols correspond to $\widetilde{W} = 0$ and $\widetilde{W} = 5.24 \times 10^{-3}$ ($W = 1.3$), respectively. The liquid bridge volume lies within the interval $0.737 \leqslant V \leqslant 0.8895$.

depending on the liquid bridge volume. This increase is around 0.03 for $V \simeq 1$, which is consistent with the numerical results shown in Fig. 5. The two liquids follow the same trend despite the large difference between the corresponding values of the Ohnesorge number, which indicates that viscosity does not significantly affect the stability limit. This result could be anticipated from the linear stability analysis because both the frequency and damping factor become zero at marginal stability (Fig. 5), and therefore the eigenmode velocity field vanishes there. However, it must be noted that the liquid bridge was not strictly at equilibrium when vibration was applied due to the finite values taken by both the vibration amplitude and frequency [38]. In fact, the dynamical effects of the upper disk vibration on the base state became more apparent as viscosity decreased. The fact that viscosity did not significantly affect the maximum slenderness in our experiments (Fig. 9) suggests that those dynamical effects do not considerably alter the liquid bridge stability.

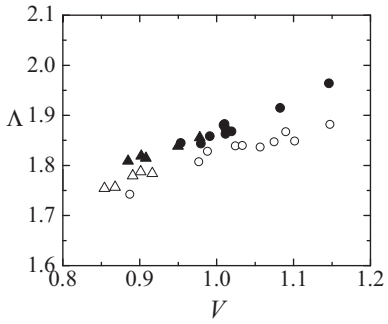

Fig. 9. Experimental values of the maximum slenderness for $\overline{B} = 0.4782$ and $\mathrm{Oh} = 6.91 \times 10^{-3}$ (triangles) and 0.237 (circles). The open and solid symbols correspond to $\widetilde{W} = 0$ and 5.24×10^{-3} ($W = 1.3$), respectively.

4.2. Breakage at the minimum volume stability limit

To conclude our analysis, we examined both experimentally and numerically the breakage of a liquid bridge at the minimum volume stability limit with and without vibration. As explained in Section. 3.2, we conducted a single experiment with an amplitude $a = 5.0$ μm and at a frequency $f = 13.2$ kHz to clearly appreciate the vibration effects on the breakage process (these conditions were not reproducible because the vibration unhooked the disk after some time). Fig. 10 shows a sequence of images right before the free surface pinching with and without vibration. As can be observed, the minimum volume decreases when the upper disk vibrates due to the stabilization effect of the induced pressure field. The initial equilibrium shape is more symmetric in this case, and so is the unstable eigenmode responsible for instability. In the nonlinear regime, a liquid thread is formed between the upper and lower parent drops. Both the gravitational force and the vibration-induced pressure field play no significant role in this phase of the breakage. The free surface pinching takes place first in the lower end of the liquid thread due to the footprint of gravity in the initial shape. The delay of the second pinching pulls up the satellite

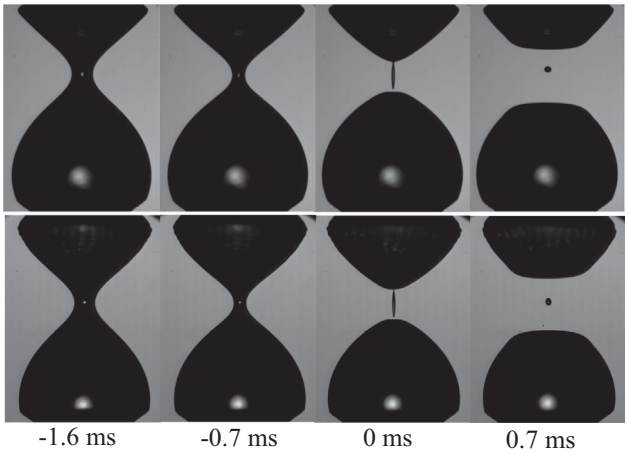

Fig. 10. Sequence of images right before the free surface pinching for $\widetilde{W} = 0$ (upper images) and 43.4×10^{-3} ($W = 3.744$) (lower images). The labels indicate the time to the pinching. The values of the rest of governing parameters are $\Lambda = 1.439, V = 0.5798$ (upper images) and 0.5448 (lower images), $B = 0.499$, and $\mathrm{Oh} = 6.91 \times 10^{-3}$.

droplet. This delay decreases in the vibrated case owing to the partial compensation of gravity. As a consequence, the satellite droplet remains suspended longer between the two parent drops. The sizes of these two parent drops are clearly affected by vibration [39]. The ratio of the upper drop volume to that of the lower drop is 0.546 and 0.218 with and without vibration, respectively, which means that vibration enhances very considerably the transfer of liquid to the upper solid surface.

Fig. 11 shows the numerical simulation of the vibrated liquid bridge breakup. The vibration-induced pressure magnitude $\frac{1}{4}|\nabla q|^2$ sharply increases near the upper triple contact line at beginning of the process. Despite its highly local character, this effect alters significantly the whole initial liquid bridge shape. The vibration-induced pressure remains confined in that very small region during breakage. For this reason, one expects that the liquid bridge evolution be essentially the same as that in absence of vibration, but starting from a different initial shape. In particular, the formation of the inner liquid thread and the free surface pinch-off are practically insensitive to the upper disk vibration. As explained in Section. 2, the simulation integrates the hydrodynamic equations asymptotically exact in the limit $A \ll 1$ and $\Omega \gg 1$. The effects associated with the finite values taken by these two quantities in the experiment are noticeable in the critical region next to the

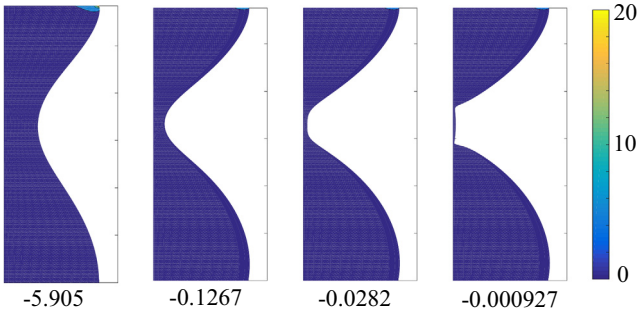

Fig. 11. Sequence of images right before the free surface pinching for $\widetilde{W} = 43.4 \times 10^{-3}$ ($W = 3.744$). The labels indicate the time to the pinching. The values of the rest of governing parameters are $\Lambda = 1.460, V = 0.5366, B = 0.505$, and $\mathrm{Oh} = 6.91 \times 10^{-3}$. These values are slightly different from those of the experiment (Fig. 10) because the latter correspond to a quasi-stable equilibrium shape, which considerably increases the CPU time.

upper triple contact line [38]. This explains the quantitative differences between the experimental and numerical results.

When a liquid drop is placed between two horizontal parallel solid surfaces, part of the drop mass can be transferred from the lower surface (donor surface) to the upper one (acceptor surface) through the quasi-static stretching and subsequent breakup of the liquid bridge formed between those surfaces. This process of mass transfer has applications in several technological fields [3]. For a small difference between the contact angles of the donor and acceptor surfaces, the triple contact lines pin on those surfaces. In this case, the process exactly corresponds to the liquid bridge breakage at its minimum volume stability limit (Fig. 10). The static transfer ratio α is defined as the ratio of volume of liquid transferred to the acceptor surface to the total liquid bridge volume after its breakup. For sufficiently small liquid bridges, the Bond number vanishes, and α becomes an intrinsic property of the system which only depends on the contact angles [41].

Consider a small liquid bridge formed between two horizontal parallel solid surfaces with the same contact angles. The liquid bridge is stretched quasi-statically until its maximum slenderness (minimum volume) stability limit is almost reached. Then, one of the surfaces is vibrated under the conditions explained in this work, while the liquid bridge is further stretched until it breaks up. The surface vibration allows one to select α by adjusting the vibration intensity $\widetilde{W}$. Fig. 12 shows the values of $\alpha(\widetilde{W})$ when either the acceptor or donor surface is vibrated. The transfer mass ratio can be significantly modified within the range of $\widetilde{W}$ considered in our experiments.

5. Concluding remarks

The stabilization of liquid bridges in air is a long-standing problem which has been approached by different means (see, e.g., Refs. [20–25]). We have shown in this work that axisymmetric millimeter liquid bridges subject to the gravitational field can be stabilized by vibrating the upper disk at a high frequency (in terms of the inverse of the capillary time) and with small amplitude (in terms of the disk radius) [40]. The liquid bridge stabilization is caused by a pressure field which produces virtually no capillary waves. In fact, if the amplitude were comparable with the liquid bridge radius (say, 100 μm), the upper disk vibration would produce large-amplitude surface waves and the phenomenon would be completely different. The liquid bridges were stabilized indefinitely, i.e., until the upper disk vibration stopped (the evaporation rate was very low). In contrast to what occurs in the stabilization by electric [23] or magnetic fields [21,22], our technique does not demand any electrical property, and can be applied to any liquid.

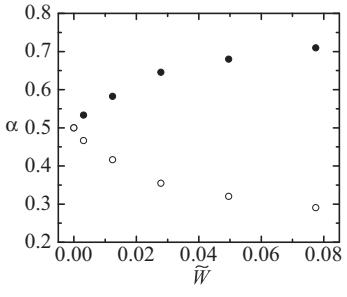

Fig. 12. Transfer mass ratio $\alpha(\widetilde{W})$ calculated from the simulation for $V = 0.545, B = 0$, and $\mathrm{Oh} = 6.91 \times 10^{-3}$ when either the acceptor (solid symbols) or donor (open symbols) surface is vibrated. In each simulation, the slenderness was that of the minimum volume stability limit with vibration.

The previous theoretical analysis [29] was restricted to configurations asymptotically close to the Plateau-Rayleigh stability limit ($\Lambda = \pi, V = 1, B = 0$). We have extended that analysis to any axisymmetric configuration by numerically solving the linearized Navier-Stokes equations. Also, we have solved the full nonlinear hydrodynamic equations to describe the liquid bridge breakup under the action of the vibration-induced pressure field.

The liquid bridge dynamics can be seen as the superposition of a fast and slow motion. The fast motion was hardly noticeable in the experiments for the Ohnesorge numbers considered, while the slow one was significantly affected by the vibration-induced pressure field. This pressure field reduces the apparent gravity force, which stands the liquid bridge upright, and consequently increases its maximum slenderness. This effect was relatively small in our experiments due to limitations of the experimental setup. In fact, oscillations of the upper disk with frequencies larger than 11 kHz unhooked it when the amplitude exceeded about 2 μm, which set an upper limit for the acoustic pressure magnitude. If this limitation is overcome, more significant effects can be obtained, and applications of this technique will become more obvious.

One of those applications is the transfer of a liquid drop from a solid surface (donor surface) to another (acceptor surface) through the stretching and breakup of liquid bridges formed between those surfaces. This mass transfer process has been used in many industrial applications, including offset printing, drop deposition, packaging industry and electronic circuits printing [3]. In the so-called *quasi-static* transfer process, the solid surfaces are moved away from each other at a speed much lower than the capillary velocity, and the bridge evolution can be seen as a series of equilibrium states. If the difference between the contact angles of the donor and acceptor surfaces is small enough, the triple contact lines pin on those surfaces, and the problem exactly corresponds to the experiment shown in Fig. 10. For sufficiently small liquid bridges, the static transfer ratio α is an intrinsic property of the system because it only depends on the contact angles [41]. The upper and lower surface vibration allows one to select α by adjusting the vibration intensity $\widetilde{W}$. For larger liquid bridges, the gravitational force becomes relevant, and the transfer ratio also depends on the Bond number, whose effective value can be controlled by the surface vibration.

The experimental analysis presented here can be extended to liquid bridges with unpinned contact lines to study the effect of the vibration-induced pressure field on the mass transfer process mentioned above. It can also be extended to both liquid lenses and pendant drops. In all these systems, one must expect a significant effect on the system's stability as long as the parameter $\widetilde{W}$ be comparable to the corresponding Bond number.

Acknowledgements

Partial support from the Ministry of Science and Education and Gobierno de Extremadura (Spain) through Grant Nos. DPI2016-78887 and GR10047, respectively, is gratefully acknowledged. We also acknowledge the support of the Mathematics Applications Consortium for Science and Industry funded by the Science Foundation Ireland Grant investigator Award No. 12/IA/1683 (www.macsi.ul.ie).

Appendix A. Supplementary material

Supplementary data associated with this article can be found, in the online version, at https://doi.org/10.1016/j.jcis.2017.11.056.

References

[1] B.N.J. Persson, Wet adhesion with application to tree frog adhesive toe pads and tires, J. Phys.: Condens. Matter. 19 (2007) 376110.
[2] A.M. Alencar, A. Majumdar, Z. Hantos, S.V. Buldyrev, H.E. Stanley, B. Suki, Crackles and instabilities during lung inflation, Physica A 357 (2005) 18–26.
[3] S. Kumar, Liquid transfer in printing processes: liquid bridges with moving contact lines, Annu. Rev. Fluid Mech. 47 (2015) 67–94.
[4] P. Suresh, I. Sreedhar, R. Vaidhiswaran, A. Venugopal, A comprehensive review on process and engineering aspects of pharmaceutical wet granulation, Chem. Eng. J. 328 (2017) 785–815.
[5] M. Dejam, H. Hassanzadeh, Z. Chen, Reinfiltration through liquid bridges formed between two matrix blocks in fractured rocks, J. Hydrol. 519 (2014) 3520–3530.
[6] J.B. Bostwick, P.H. Steen, Stability of constrained capillary surfaces, Annu. Rev. Fluid Mech. 47 (2015) 539–568.
[7] L. Rayleigh, On the instability of jets, Proc. London Math. Soc. s1-10 (1878) 4–13.
[8] H.C. Kuhlmann, Thermocapillary Convection in Models of Crystal Growth, Springer-Verlag, Berlin, 1999.
[9] S. Dodds, M. Carvalho, S. Kumar, Stretching and slipping of liquid bridges near plates and cavities, Phys. Fluids 21 (2009) 092103.
[10] M. Prakash, D. Quéré, J.W.M. Bush, Surface tension transport of prey by feeding shorebirds: the capillary ratchet, Science 320 (2008) 931–934.
[11] A.K. Uguza, N.J. Alvarez, R. Narayanan, An experimental study on the instability of elliptical liquid bridges, Phys. Fluids 17 (2005) 078106.
[12] S. Sankaran, D.A. Saville, Experiments on the stability of a liquid bridge in an axial electric field, Phys. Fluids 5 (1993) 1081–1083.
[13] A. Ramos, H. González, A. Castellanos, Experiments on dielectric liquid bridges subjected to axial electric fields, Phys. Fluids 6 (1994) 3206–3208.
[14] M.J. Marr-Lyon, D.B. Thiessen, P.L. Marston, Stabilization of a cylindrical capillary bridge far beyond the Rayleigh-Plateau limit using acoustic radiation pressure and active feedback, J. Fluid Mech. 351 (1997) 345–357.
[15] A. Casner, J.-P. Delville, Laser-sustained liquid bridges, Europhys. Lett. 65 (2004) 337–343.
[16] M.P. Mahajan, M. Tsige, P.L. Taylor, C. Rosenblatt, Stability of liquid crystalline bridges, Phys. Fluids 11 (1999) 491–493.
[17] B.J. Lowry, P.H. Steen, Stabilization of an axisymmetric liquid bridge by viscous flow, Int. J. Multiphase Flow 20 (1994) 439–443.
[18] B.J. Lowry, P.H. Steen, Stability of slender liquid bridges subjected to axial flows, J. Fluid Mech. 330 (1997) 189–213.
[19] A.K. Uguz, N. Alvarez, R. Narayanan, An experimental study of the stability of liquid bridges subject to shear-induced closed-flow, J. Colloid Interface Sci. 346 (2010) 464–469.
[20] J. Meseguer, L.A. Slobozhanin, J.M. Perales, A review on the stability of liquid bridges, Adv. Space Res. 16 (1995) 5–14.
[21] M.P. Mahajan, M. Tsige, P.L. Taylor, C. Rosenblatt, Paramagnetic liquid bridge in a gravity-compensating magnetic field, Phys. Fluids 10 (1998) 2208–2211.
[22] M.P. Mahajan, S. Zhang, M. Tsige, P.L. Taylor, C. Rosenblatt, Stability of magnetically levitated liquid bridges of arbitrary volume subjected to axial and lateral gravity, J. Colloid Interface Sci. 213 (1999) 592–595.
[23] N.A. Pelekasis, K. Economou, J.A. Tsamopoulos, Linear oscillations and stability of a liquid bridge in an axial electric field, Phys. Fluids 13 (2001) 3564–3581.
[24] M.J. Marr-Lyon, D.B. Thiessen, P.L. Marston, Passive stabilization of capillary bridges in air with acoustic radiation pressure, Phys. Rev. Lett. 86 (2001) 2293–2296.
[25] D.B. Thiessen, M.J. Marr-Lyon, P.L. Marston, Active electrostatic stabilization of liquid bridges in low gravity, J. Fluid Mech. 457 (2002) 285–294.
[26] M.A. Herrada, J.M. López-Herrera, E.J. Vega, J.M. Montanero, Numerical simulation of a liquid bridge in a coaxial gas flow, Phys. Fluids 23 (2011) 012101.
[27] Y. Gaponenko, A. Mialdun, V. Shevtsova, Shear driven two-phase flows in vertical cylindrical duct, Int. J. Multiphase Flow 39 (2012) 205–215.
[28] J.M. Montanero, C. Ferrera, V.M. Shevtsova, Experimental study of the free surface deformation due to thermal convection in liquid bridges, Exp. Fluids 45 (2008) 1087–1101.
[29] E.S. Benilov, Stability of a liquid bridge under vibration, Phys. Rev. E 93 (2016) 063118.
[30] M.A. Herrada, J.M. Montanero, A numerical method to study the dynamics of capillary fluid systems, J. Comput. Phys. 306 (2016) 137–147.
[31] E.J. Vega, J.M. Montanero, C. Ferrera, Exploring the precision of backlight optical imaging in microfluidics close to the diffraction limit, Measurement 44 (2011) 1300–1311.
[32] A. Ponce-Torres, E.J. Vega, J.M. Montanero, Effects of surface-active impurities on the liquid bridge dynamics, Exp. Fluids 57 (2016) 67.
[33] M.G. Cabezas, A. Bateni, J.M. Montanero, A.W. Neumann, A new method of image processing in the analysis of axisymmetric drop shapes, Colloids Surf. A 255 (2005) 193–200.
[34] M.G. Cabezas, A. Bateni, J.M. Montanero, A.W. Neumann, Determination of surface tension and contact angle from the shapes of axisymmetric fluid interfaces without use of apex coordinates, Langmuir 22 (2006) 10053–10060.
[35] L.A. Slobozhanin, J.M. Perales, Stability of liquid bridges between equal disks in an axial gravity field, Phys. Fluids 5 (1993) 1305–1314.

[36] A. Ponce-Torres, M.A. Herrada, J.M. Montanero, J.M. Vega, Linear and nonlinear dynamics of an insoluble surfactant-laden liquid bridge, Phys. Fluids 28 (2016) 112103.
[37] J.A. Nicolás, J.M. Vega, Linear oscillations of axisymmetric viscous liquid bridges, Z. Angew. Math. Phys. 51 (2000) 701–731.
[38] The Supplemental Material includes a video which shows the superposition of the slow motion and the fast one due to the finite values taken by the vibration amplitude and frequency. The slow motion corresponds to the damping of a perturbation introduced at a certain instant, and its characteristic time commensurates with the capillary time. The fast motion manifests itself through the ripples traveling over the free surface.
[39] The Supplemental Material includes a video which shows the breakage processes in Fig. 10.
[40] The Supplemental Material includes a video which shows how a liquid bridge stabilized by the upper disk vibration breaks up when that vibration stops. One can distinguish two phases. First, the liquid bridge adopts a new quasi-static shape, and then breaks up because that shape is unstable.
[41] H. Chen, T. Tang, A. Amirfazli, Mechanism of liquid transfer between two surfaces and the role of contact angles, Soft Matter 10 (2014) 2503–2507.